Sustainable Hydrothermal Synthesis of Zeolite A as an Alternative to Commercial Molecular Sieves for Moisture Adsorption in Oil and Gas Processing

Meyliana Wulandari[1*], Nesya Juniar[2], Wawan Rustyawan[3], Stella Jovita[4], Pandian Bothi Raja[5], and Nofrizal Nofrizal[6]

[1]*Department of Chemistry, Faculty of Mathematics and Natural Sciences, Universitas Negeri Jakarta, Jl. Rawamangun Muka, Jakarta Timur 13220, Indonesia*

[2]*Department of Chemistry Education, Faculty of Educational Sciences, State Islamic University (UIN) Syarif Hidyatullah Jakarta, Jl. Ir H. Juanda No. 95, Banten 15412, Indonesia*

[3]*Research and Technology Innovation, Pertamina, Jl. Raya Bekasi, Jakarta Timur 13820, Indonesia*

[4]*Department of Chemistry, Faculty of Science and Data Analytics, Institut Teknologi Sepuluh Nopember, Jl. Raya ITS, Keputih, Sukolilo, Surabaya 60111, Indonesia*

[5]*School of Chemical Sciences, Universiti Sains Malaysia, 11800 Minden, Penang, Malaysia*

[6]*Research and Development Center for Oil and Gas Technology – Lemigas, Jl. Ciledug Raya Kavling 109, Jakarta 12230, Indonesia*

* ***Corresponding author:***

email: meyliana.wulandari@unj.ac.id

Received: August 27, 2025
Accepted: December 16, 2025

DOI: 10.22146/ijc.110739

Abstract: *The presence of water during downstream oil and gas production can cause corrosion and blockages through reactions with CO_2 and H_2S. Zeolites are effective desiccants for moisture adsorption due to their microporous aluminosilicate framework. In this study, zeolite A was synthesized hydrothermally by varying the Si/Al molar ratio (0.80, 1.14, 1.80) and temperature (70, 100, 130 °C) to identify the optimal conditions for moisture adsorption. XRD analysis revealed that the zeolite synthesized at a Si/Al ratio of 1.14 and 130 °C achieved the highest crystallinity (97%), comparable to commercial molecular sieve A. Surface area analysis (BET) showed that this synthesized zeolite exhibited a surface area of 127.48 m^2/g and a pore diameter of 53 Å. The adsorption capacity test in a humidity chamber demonstrated a value of 0.188 ppmv for the synthesized zeolite, compared to 1.101 ppmv for the commercial molecular sieve. The lower adsorption efficiency was attributed to reduced surface area, incomplete crystallinity, and diffusion limitations. Nevertheless, the optimized synthesis route produced zeolite A with desirable structural and textural properties, offering a cost-effective and environmentally friendly alternative desiccant for gas dehydration applications in the oil and gas industry.*

Keywords: *hydrothermal; molecular sieve; moisture adsorption; zeolite*

■ INTRODUCTION

A common issue in the production of crude oil and natural gas is the presence of water, which can lead to problems in the transportation process and operations in the downstream sector [1]. Water in the system can react with CO_2 and H_2S to form acids [2], causing corrosion [3]. In addition, water can form hydrates or solids that cause blockages in transportation pipes [4]. Hence, water needs to be removed by a dehydration process. The dehydration process is carried out to remove water vapor from the gas stream at a low temperature, where the water will condense. This temperature is referred to as the dew point [5]. Suitable adsorbents for adsorbing water include glycerol and porous solids. Glycerol is unable to absorb water levels lower than 0.1 ppmv at dew point conditions of -80 to -100 °C required in the natural

gas industry. Additionally, glycerol causes corrosion when its viscosity is high [6].

Over the past four decades, various adsorbents have been developed and tested for water vapor removal, including silica gel, molecular sieves (3A, 4A, 5A, 13X), anhydrous $CaSO_4$ (Drierite), and activated alumina. Among these adsorbents, molecular sieve is the first choice for adsorbents in the dehydration process because it can absorb water content < 0.1 ppmv [7]. Molecular sieves are important compounds that can be used as desiccant materials in the gas industry. One of the commonly used desiccant materials is zeolite, which is a crystalline material with a porous structure in the nanoscale range and a three-dimensional framework composed of tetrahedral aluminosilicate, as well as charge-balancing ions that can be exchanged on its surface [8]. These characteristics make zeolite able to act as a water-absorbing molecule because it has a porous material that allows smaller molecules like water to be absorbed in the zeolite pores [9].

Zeolites used for natural gas adsorption can be synthesized using solvents in solvothermal, hydrothermal, and ionothermal methods. The solvothermal method uses organic solvents, such as alcohols (methanol, ethanol, amyl alcohol), ethylene glycol, hydrocarbons, and pyridine. In contrast to the solvothermal method, the hydrothermal method uses water as a solvent, while the ionothermal method uses ionic solutions. Synthesis using the solvothermal method has many advantages. However, when organic solvents are used in this method, they have the potential to cause negative environmental impacts. Conversely, the hydrothermal method is considered environmentally friendly because it uses water as a solvent [10].

The performance of zeolites in water vapor adsorption applications depends on their surface area and hydrophilic or hydrophobic properties, which are directly influenced by the Si/Al ratio and the presence of hydroxyl groups [11]. Zeolites can be obtained from natural materials or chemically synthesized in the laboratory. The use of zeolites from natural materials is limited by the fact that mineral deposits are often of low quality, containing only around 15–20% zeolite, whereas deposits with high purity have a zeolite content of 90–95%. The presence of impurities in natural zeolites can interfere with the formation of zeolite crystal aggregates; therefore, these impurities must be removed through a purification process. However, this process requires relatively high costs [12]. Therefore, the synthesis of zeolites in the laboratory is a more controlled alternative and can be adjusted to the specifications and structure required as a molecular sieve [13].

Previous studies have successfully reported the synthesis and performance of zeolite type 4A (Linde Type A, LTA) and natural zeolite chabazite (CHA) as gas-phase moisture adsorbents. That study reported the optimum Si/Al ratios for LTA and CHA were 1.34 and 3.05, respectively and the adsorption activity test results showed that LTA samples containing Na^+ exhibited a much lower nitrogen adsorption capacity than CHA containing Ca^{2+}. It occurs due to kinetic restrictions on the diffusion of nitrogen molecules in LTA zeolite [14]. Moura et al. reported the successful synthesis of type 4A (LTA) and also showed that the Si/Al ratio did not affect crystallinity. However, the presence of large amounts of potassium could cause the zeolite structure to become amorphous. It provides information that the presence of Na^+ has the highest water adsorption [9]. Other studies have reported the synthesis of zeolites for water adsorption, including the synthesis of zeolite 13X used for water adsorption by Wynnyk et al. which employed the hydrothermal method. The results of energy dispersive X-ray spectroscopy (EDX) measurements showed that the synthesized zeolite 13X particles had an average diameter of 21.41 μm with a Si/Al ratio of 1.8 [15]. In addition to synthesizing 13X, Wynnyk et al. [16] have successfully reported the synthesis of zeolite 4A carried out by the hydrothermal method. This study produced crystal micrographs of zeolite samples with a beveled cube shape in analysis using a scanning electron microscope (SEM).

From the synthesis perspective, the hydrothermal method for producing zeolite A with varying Si/Al ratios has been extensively reported in the literature. The investigation of the effect of the Si/Al molar ratio on zeolite synthesis using natural and waste-based

precursors, such as nipah leaf silica and used canned aluminum, has been reported. Their work demonstrated that the Si/Al ratio significantly influences the crystallinity and phase purity of the resulting zeolite. However, most existing studies focus on alternative silica or alumina sources rather than optimizing hydrothermal conditions (e.g., temperature and Si/Al ratio) specifically for zeolite A intended for moisture adsorption applications in natural gas systems [17]. Another study successfully synthesized zeolite A from industrial fly ash as a green and cost-effective adsorbent for the removal of Cd^{2+} and Pb^{2+} in wastewater applications. Their results demonstrated that the Si/Al ratio strongly affects zeolite crystallinity and adsorption efficiency. However, most previous studies, including those focused on wastewater treatment or ion exchange applications, have not systematically optimized both the Si/Al ratio and hydrothermal temperature for zeolite A intended as a molecular sieve in gas-phase moisture adsorption [18].

The investigation of the effects of synthesis parameters on the formation of zeolite 4A crystals and evaluated their performance for heavy-metal uptake in water treatment applications has been reported. Their findings confirmed that factors such as the Si/Al ratio and alkalinity significantly influence the morphology and crystallinity of zeolite 4A [19]. The synthesis of zeolite as a molecular sieve component by varying the Si/Al molar ratio has been carried out for bauxite [20]. Other research has also reported the use of a Si/Al molar ratio of 1 with synthesis temperatures of 60, 80 and 100 °C [15], as well as a Si/Al ratio of 1 at 90 °C, which was not further applied to a humidity chamber [21]. Whereas the present work aims to optimize the Si/Al ratio and hydrothermal temperature to enhance zeolite A performance as a molecular sieve desiccant for moisture adsorption in natural gas.

In this study, zeolite synthesis was carried out by varying the Si/Al molar ratio and hydrothermal temperature to determine the optimal conditions for zeolite as a molecular sieve component for water adsorbent agents in natural gas. The variations in the Si/Al molar ratio were 1.14, 1.80, and 0.80, and temperatures of 70, 100, and 130 °C. The best zeolite is expected to be applied to the water adsorption process on natural gas samples with a humidity chamber. The hydrothermal synthesis route employed in this study offers significant advantages in terms of cost efficiency, environmental sustainability, and operational simplicity. The hydrothermal method uses water as a solvent, making it a greener and safer approach. This minimizes chemical waste generation and reduces environmental impact, aligning the process with the principles of green chemistry. Additionally, the synthesis is conducted at a moderate temperature (130 °C) and short crystallization time (4 h), which significantly reduces energy consumption and processing costs compared to conventional methods that often require higher temperatures and longer durations.

■ EXPERIMENTAL SECTION

Materials

The materials used in this study were purchased from Merck Germany (99% purity), including: sodium aluminate ($NaAlO_2$), sodium silicate (Na_2SiO_3), sodium hydroxide (NaOH), and boric acid (H_3BO_3).

Instrumentation

The tools used in this research include glassware commonly used in chemistry laboratories. The instruments used include X-ray diffraction (XRD, Empyrean), SEM (Jeol JSM-IT200), surface area analyzer (SAA, AUTOSORB-6B), and X-ray fluorescence (XRF, Axios).

Procedure

Zeolite synthesis

The initial stage in synthesizing zeolite is the preparation stage, which involves dissolving NaOH in water, and then transferring the solution to a propylene bottle [22]. The first bottle is filled with $NaAlO_2$ and shaken until transparent; the second bottle is filled with sodium metasilicate and shaken until transparent and completely dissolved. Both mixtures are made with a molar ratio of Si/Al of 1.14, 1.80, and 0.80. Next, the silica solution is poured into the alumina solution quickly until a thick gel forms. Both solutions are stirred until homogeneous. The next stage involves crystallizing

Table 1. Sample code

Ratio	Temperature		
	70 °C	100 °C	130 °C
1.14	NaA–1.14–70	NaA–1.14–100	NaA–1.14–130
1.80	NaA–1.8–70	NaA–1.8–100	NaA–1.8–100
0.80	NaA–0.8–70	NaA–0.8–100	NaA–0.8–130

the mixture at various temperatures, namely 70, 100, and 130 °C, for 4 h (Table 1). After crystallization, the reaction mixture is cooled to a temperature below 30 °C, filtered, washed with water to reach a pH below 9, and dried at a constant temperature of 110 °C until dry.

Characterization of zeolite

Zeolite crystallinity was analyzed using XRD. The synthesized zeolite was ground and sieved to a size of 200 mesh. The sample was placed in a holder, pressed and flattened, and measurements were taken at an angle of 2θ between 5° and 50° at a voltage of 40 kV and a current of 15 mA. Intensities were generated and plotted on the y-axis [23]. The resulting pattern was processed using OriginPro 2024 software (64-bit) to determine the crystallinity of the zeolite sample. The degree of crystallinity was calculated using the Gaussian-Lorentzian function in Eq. (1) [24]:

$$X_c = \frac{A_c}{A_c + A_a} \times 100\% \quad (1)$$

where, X_c = crystallinity (%), A_c = crystalline peak diffraction area, A_a = amorphous peak diffraction area

SEM-EDX analysis was performed to study the surface morphology and %atomic composition. Zeolite was cleaned with isopropanol, then dried and stored in a desiccator. The data obtained were then processed with the ImageJ software. Meanwhile, in XRF analysis, 10 g of the sample was ground into fine particles, and then a binder mixture was added. The mixture was then subjected to a hydraulic pressure of 10–40 T. Quantitative component measurements were performed at a voltage of 40 kV and a current of 45 mA [25]. The SAA instrument uses N_2 gas to produce data on surface area, volume, and pore diameter [26]. The sample tube containing the filler was closed and weighed empty. Furthermore, 0.2 g of the sample was placed in a tube and filled with filler, then degassed at 100 °C for 2 h and at 300 °C for 3 h. After that, the sample tube was weighed again. The sample tube was then attached to the analysis port and flowed through a mixture of helium and nitrogen gas. The analysis results were obtained in the form of an N_2 adsorption-desorption curve, which can be used to determine the surface area (m^2/g), pore volume (cc/g), and pore diameter (Å).

Zeolite Characterization using XRF follows the ASTM D7343 method. Zeolite powder was placed in a special aluminum mold and compressed using a press until it was compacted. The sample was then placed in an XRF container and analyzed at 40 kV and 45 mA using a quantitative analysis program. The results were calculated as the percentage of zeolite content.

Zeolite application for moisture adsorption

The application of zeolite as a molecular sieve component agent was conducted using a compact humidity chamber at 30 °C and a pressure of 7 kg f/cm^2 to determine its adsorption capacity. A total of 1 L of gas was flowed into the humidity chamber containing zeolite. The test was carried out by weighing the zeolite before and after being inserted into the chamber after 1 h of adsorption. The adsorption capacity was calculated using Eq. (2);

$$Q\ (\%) = \frac{(w_3 - w_2)}{w_2} \times 100\% \quad (2)$$

where, Q (%) = Adsorption capacity (%), w_3 = final mass (g), w_2 = initial mass (g)

After calculating the adsorption capacity, the next step is to determine the ppmv using Eq. (3).

$$\text{ppmv} = \left(\frac{\text{Adsorption\%}}{100}\right)\left(\frac{\text{adsorbed gas volume}}{\text{total gas volume}}\right) \times 10^6 \quad (3)$$

■ RESULTS AND DISCUSSION

Gel Formation Behavior of Zeolite

In this study, zeolite was made from $NaAlO_2$, Na_2SiO_3, NaOH, and H_2O [27]. The zeolite synthesis in this study was carried out with a material composition based on Mintova's experiment, namely a Si/Al ratio of 1 at a molar composition ratio of Si/Al of 1.14; a molar ratio of Si/Al of 1.8; and a molar ratio of Si/Al of 0.8. The synthesis process began by reacting $NaAlO_2$, Na_2SiO_3,

and NaOH solution. NaOH plays a crucial role in the formation of zeolite during the crystallization process, as Na^+ cations are utilized to stabilize the zeolite framework [28]. The resulting mixture was then homogenized at room temperature to form a white gel mixture. Gel formation indicates the interaction between aluminate and silicate in the formation of nuclei and the growth of zeolite crystals [29]. Based on previous research, this mixture contains an amorphous phase [30].

Zeolite synthesis is generally carried out in alkaline conditions because Na_2SiO_3 and $NaAlO_2$ are completely soluble in alkaline conditions (Eq. (4)). In zeolite synthesis, OH^- ions produced from alkali salts are known as demineralizing agents that play a role in increasing the solubility of silica and alumina compounds, thus producing aluminate and silicate ions. Additionally, alkali salts serve as a source of inorganic cations [31]. During the hydrothermal process, the amorphous gel will change with the rearrangement of the zeolite structure so that crystal nuclei and a regular zeolite structure with strong bonds will be formed [17].

$$Na_2SiO_{3(l)} + 2NaAlO_{2(l)} \xrightarrow{\text{hydrothermal}} \left[Na_x(AlO_2)_y(SiO_2)z \cdot NaOH \cdot H_2O\right]_{(crystal)} \quad (4)$$

The resulting white gel was then washed and demineralized to a pH of < 9 to remove any remaining NaOH. The cleaned gel was then dried at 110 °C. The final product of this zeolite synthesis process was a white powder.

Measurement of the Degree of Crystallinity of Zeolites Using XRD

The diffractogram (arrangement of lines with intensity and position 2θ) of zeolite is shown in Fig. 1. The purpose of this characterization is to determine the optimum conditions of temperature variations (70, 100, and 130 °C and the molar ratio of Si/Al (1.14, 1.80, and 0.80). The results of the zeolite A identification were then compared with those of ICDD and molecular sieve A (Table 2 and Fig. 1). The results show that there are 10 major peaks in 1(a), 1(b), 1(c), 1(e), and 1(f), indicating zeolite A with a high crystalline phase. However, in Fig. 1 (plots 1(d), 1(g), 1(h), and 1(i)), the diffraction pattern of zeolite A is not produced, indicating that the zeolite in the amorphous phase has not transformed into a crystalline phase [32]. These results were confirmed based on previous research, which reported that zeolite A was formed when a specific peak appeared in the 2θ

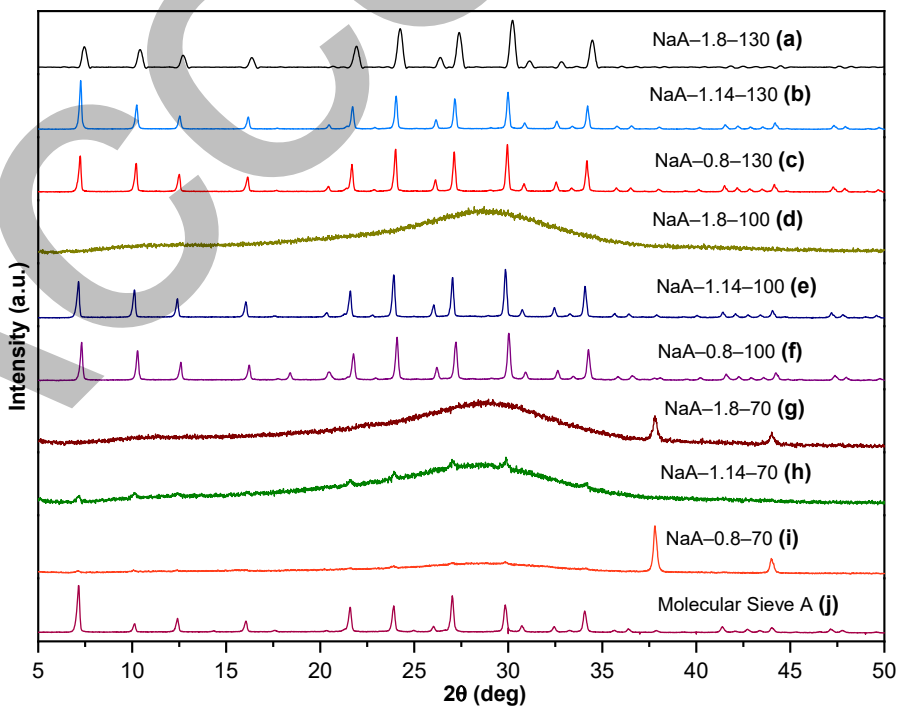

Fig 1. XRD diffraction of zeolite (temperature and Si/Al molar ratio optimization)

Table 1. Diffraction angle of synthesized zeolite and molecular sieve A

Sample	2θ (°)	Crystallinity (%)
NaA–0.8–70 (i)	37.80, 44.00	8
NaA–1.14–70 (h)	21.57, 23.96, 26.50	12
NaA–1.8–70 (g)	29.03, 37.79, 44.00	11
NaA–0.8–100 (f)	7.32, 10.29, 12.58, 16.23, 21.77, 24.09, 26.20, 27.21, 30.02, 34.26	93
NaA–1.14–100 (e)	7.15, 10.12, 12.41, 16.05, 21.59, 23.91, 26.04, 27.03, 29.85, 34.09	96
NaA–1.8–100 (d)	28.60	14
NaA–0.8–130 (c)	7.24, 10.21, 12.51, 16.15, 21.69, 24.01, 26.13, 27.13, 29.95, 34.18	95
NaA–1.14–130 (b)	7.27, 10.24, 12.52, 16.17, 21.72, 24.03, 26.16, 27.16, 29.98, 34.21	97
NaA–1.8–130 (a)	7.35, 10.31, 12.58, 16.25, 21.80, 24.13, 26.27, 27.26, 30.23, 34.46	40
Molecular sieve A (j)	7.16, 10.12, 12.41, 16.05, 21.58, 23.90, 26.02, 27.02, 29.83, 34.05	100

diffractogram between 7° and 16°, namely at 7.20°, 10.19°, 12.49°, and 16.14° [33]. In addition, the success of the synthesis was also seen by comparing the data obtained with standard data, namely International Center for Diffraction Data (ICDD). Based on ICDD No. 00–038–0241, zeolite A, which was successfully synthesized, was found in samples with temperatures of 100 and 130 °C, and at Si/Al molar ratios of 0.80; 1.14; and 1.80 (Fig. 1(a), 1(b), 1(c), 1(e), and 1(f)). These results are also in accordance with previous research, which reported the results of XRD analysis for zeolite A at 2θ, namely 7.2°, 10.1°, 12.4°, 16.2°, 21.6°, 24.0°, 26.0°, 27.0°, 30.0°, 34.0°, showing an XRD pattern with a high crystalline phase [18].

Fig. 1(i) shows a zeolite synthesized using a Si/Al molar ratio of 0.8 at a temperature of 70 °C, exhibiting peaks at 2θ angles of 37.80° and 44.00°, as listed in Table 2. When compared with the reference zeolite molecular sieve A, the zeolite synthesized 1i is not zeolite A. Fig. 1(f) is a zeolite synthesized with a Si/Al molar ratio of 0.8, showing peaks at 2θ: 7.32°, 10.29°, 12.58°, 16.23°, 21.77°, 24.09°, 26.20°, 27.21°, 30.02°, 34.26°. The diffraction angle of sample f gives a diffraction pattern of zeolite molecular sieve A, so it can be concluded that zeolite 1(f) is zeolite A. In the same way, the synthesized zeolites listed in Table 2 can be classified as zeolite 1(d), 1(g), 1(h), and 1(i), which are not zeolite A. It shows that the synthesis of zeolite A was successfully carried out at temperatures above 90 °C with all Si/Al molar ratios of 0.80, 1.14, and 1.80. Previous studies confirmed the XRD results of zeolite A in this study, showing that zeolite synthesized at temperatures above 90 °C can produce zeolite [34]. The results of XRD analysis can also be used to calculate crystallinity, allowing for the best variation of the synthesized zeolite to be seen in Table 2.

Zeolite crystallinity is shown in Table 2. The highest crystallinity is shown by the Si/Al ratio of 1.14 and a temperature of 130 °C, and is close to molecular sieve A. The results show that an increase in hydrothermal temperature can affect crystallinity. It is because the growth rate and nucleation rate increase [35]. The zeolite formed is influenced by the reaction temperature, so that a low crystallization temperature results in a percentage of crystallinity [34]. It has been previously studied and reported that increasing the synthesis temperature parameter will increase crystallinity. Meanwhile, increasing the reactant ratio will reduce crystallinity [33-34].

Analysis of The Morphology of Zeolite Using SEM-EDX

Based on the SEM micrographs in Fig. 2, the synthesized zeolite exhibits a distinct cube-shaped morphology, which is a characteristic feature of zeolite A (LTA-type) crystals. The observation of three different cube forms confirms that the product belongs to the zeolite A structural family, as this morphology is consistent with previously reported standard shapes of zeolite A crystals [19]. In Fig. 2(d) and 2(g), the zeolite particles appear as cubes with rounded edges, while in Fig. 2(e) and 2(h), the crystals show truncated or cut edges, and in Fig. 2(i), the cubes possess well-defined sharp edges.

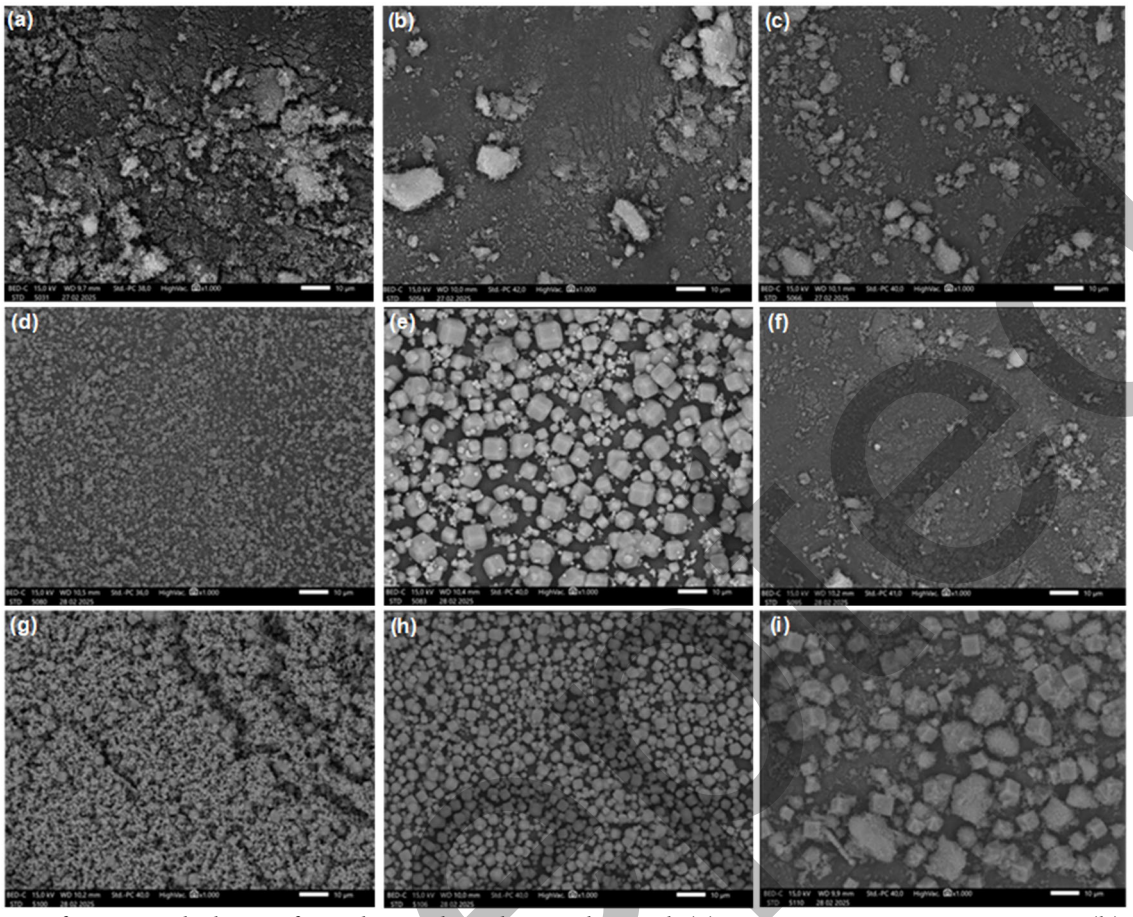

Fig 2. The surface morphology of synthesized zeolite with Si/Al (a) ratio 0.8 temperature 70 °C, (b) ratio 1.14 temperature 70 °C, (c) ratio 1.8 temperature 70 °C, (d) ratio 0.8 temperature 100 °C, (e) ratio 1.14 temperature 100 °C, (f) ratio 1.8 temperature 100 °C, (g) ratio 0.8 temperature 130 °C, (h) ratio 1.14 temperature 130 °C, (i) ratio 1.8 temperature 130 °C

These variations in edge sharpness indicate differences in crystal growth conditions, particularly related to alkalinity and supersaturation during synthesis. The formation of rounded-edged crystals (Fig. 2(d) and 2(g)) can be attributed to conditions of high alkalinity and high supersaturation, which promote rapid nucleation and hinder the development of well-defined crystal facets [36]. Under such conditions, the concentration of aluminum species in the reaction mixture is relatively high, leading to the formation of numerous nuclei in a short time. As synthesis progresses, these nuclei continue to grow while consuming the available aluminum in the gel. Consequently, the aluminum content becomes depleted, leading to irregular crystal growth and the appearance of rounded or distorted edges.

In contrast, when the alkalinity and supersaturation are moderate, the rate of nucleation is balanced with the growth rate, allowing crystals to develop more uniform and faceted shapes. This results in cubes with truncated or cut edges (Fig. 2(e) and 2(h)). Under more controlled growth conditions, where nucleation is less dominant, and crystal growth is gradual, sharp-edged cubic crystals (Fig. 2(i)) are obtained. These sharp, well-defined morphologies indicate a stable growth environment where silicate and aluminate species are available in optimal proportions for zeolite A formation.

The SEM morphological observations are consistent with the XRD analysis, which confirmed that the samples possess a high degree of crystallinity. The

presence of well-defined cubic crystals with varying edge sharpness is shown in Fig. 2(d), 2(e), 2(g), 2(h), and 2(i) further support that the synthesized material is crystalline zeolite A. The morphological differences among these samples reflect the influence of synthesis parameters—particularly alkalinity, pH, and the Si/Al ratio—on crystal growth behavior and surface development. On the other hand, Fig. 2(a), 2(b), 2(c), and 2(f) have irregular shapes, indicating that the particles are still amorphous. It can be concluded that zeolite synthesis is influenced by crystallization temperature; higher temperatures result in crystals with faster growth rates. The results obtained are that zeolites with synthesis temperatures above 100 °C can form zeolites in a synthesis time of 4 h in accordance with previous studies [25].

Table 3 shows that the synthesized zeolite consists of the main components, namely Na, Al, Si, and O. At the same temperature, increasing the initial Si/Al ratio at the beginning of the synthesis results in an increasing Si/Al ratio in the final sample. Increasing the Si/Al ratio in the initial synthesis material makes silica dissolution more optimal, resulting in an increased silica concentration in the solution. Silica that continues to increase will cause the phenomenon where silica is unable to enter the zeolite structure, resulting in precipitation as an amorphous phase, which leads to a decrease in the crystallinity of the synthesized product [37]. It can be seen in Fig. 2(i) that the highest Si/Al ratio, namely 1.8, still contains amorphous material attached to the zeolite cube.

At the same ratio with different synthesis temperatures, it provides different Si/Al ratio information, namely, there is a decrease in the Si/Al ratio from 70 to 100 °C for all ratios, namely, 0.80; 1.14; and 1.80. However, there is an increase in the Si/Al ratio again at 130 °C, but only at the Si/Al ratio of 1.14, which does not experience a change in the ratio when the temperature increases to 130 °C. This indicates that 100 °C is the optimum temperature for the synthesis of zeolite A because this decrease in the Si/Al ratio indicates that silica or alumina enters the zeolite structure. It is in line with previous research [38]. The results show that the largest Al mass percentage is in the sample with a Si/Al ratio of 0.8, as indicated by its SEM morphology, resulting in cubic crystals with rounded edges. Fig. 3 shows the particle size distribution of zeolite A synthesized using Si/Al ratios of 0.80, 1.14, and 1.80 at temperatures of 100 and 130 °C The particle size ranges from 0.5 to 8.0 μm. This result is supported by previous research, reporting the zeolite's particle size distribution in the range of 2 to 50 μm [35-36].

Table 3. EDX analysis of zeolite

Sample	Atomic %			
	O	Na	Al	Si
NaA–0.8–70 (a)	64.80	12.41	11.44	11.35
NaA–1.14–70 (b)	65.94	11.18	10.96	11.92
NaA–1.8–70 (c)	64.81	11.07	10.94	13.18
NaA–0.8–100 (d)	64.88	12.26	12.03	10.84
NaA–1.14–100 (e)	62.03	13.08	12.55	12.35
NaA–1.8–100 (f)	70.47	10.43	8.89	10.20
NaA–0.8–130 (g)	60.77	12.75	13.62	12.86
NaA–1.14–130 (h)	62.58	12.84	12.41	12.17
NaA–1.8–130 (i)	61.25	11.89	12.18	14.68

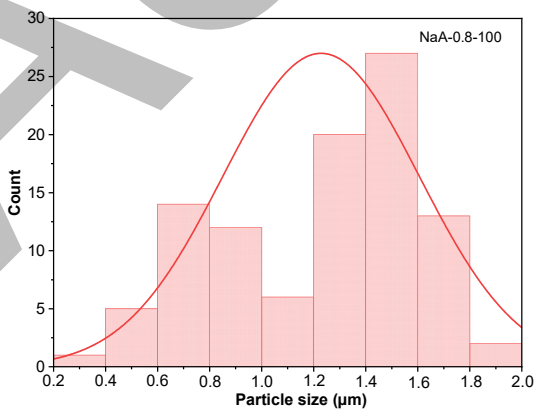

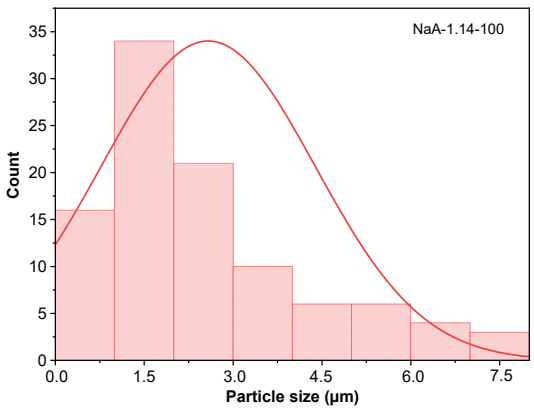

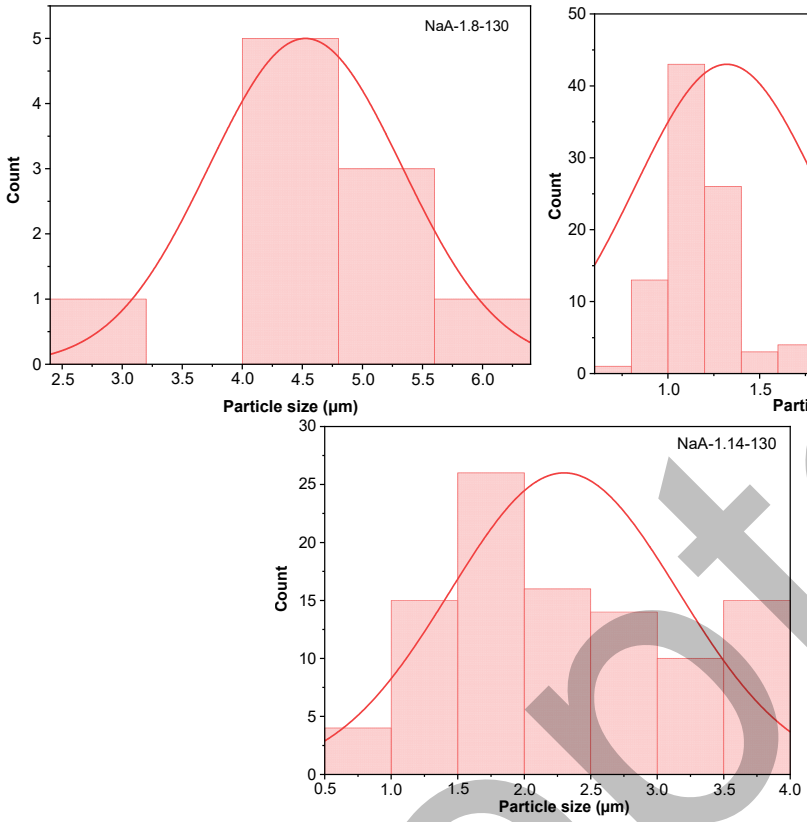

Fig 3. Particle size distribution of zeolite A synthesized using Si/Al ratios of 0.80, 1.14, and 1.80 at temperatures of 100 and 130 °C

Table 4. Surface area, pore diameter, and pore volume of synthesized zeolite A

Sample code	Surface area (m^2/g)	Pore volume (cc/g)	Pore diameter (Å)
NaA–0.8–70	48.820	0.070	63
NaA–1.14–70	80.350	0.100	90
NaA–1.8–70	70.930	0.150	85
NaA–0.8–100	8.560	0.010	74
NaA–1.14–100	2.720	0.003	44
NaA–1.8–100	68.830	0.130	77
NaA–0.8–130	4.120	0.007	72
NaA–1.14–130	127.480	0.170	53
NaA–1.8–130	42.200	0.040	41
Molecular sieve A [40]	288.210	0.170	17

Analysis of Surface Area, Pore Diameter, and Pore Volume of Zeolite

The surface area, pore diameter, and pore volume of the synthesized zeolites were characterized using a surface area analyzer (SAA) instrument based on the BET method (Table 4). The data indicate that at a synthesis temperature of 70 °C, increasing the Si/Al molar ratio results in a progressive increase in surface area. This trend suggests that a higher Si/Al ratio promotes the formation of a more open zeolite framework, characterized by a larger number of accessible micropores and active adsorption sites. The substitution of Al^{3+} with Si^{4+} reduces the framework charge density, thereby decreasing the concentration of charge-balancing cations (Na^+) in the pores and increasing pore accessibility.

Conversely, synthesis temperature exerts a significant influence on the resulting surface area. For instance, at a Si/Al ratio of 0.8, the surface area decreases markedly from 48.82 m^2/g at 70 °C to 8.56 m^2/g at 100 °C and further to 4.12 m^2/g at 130 °C. A similar declining trend is observed for other Si/Al ratios, indicating that excessive hydrothermal temperatures may cause partial collapse or sintering of the zeolite framework, thereby reducing the number of open pores available for adsorption. This behavior aligns with previous findings [39], which reported that elevated synthesis temperatures can accelerate nucleation and crystal growth, but may also lead to pore coalescence and a reduction in specific surface area.

Generally, a larger surface area corresponds to a greater adsorption capacity because more adsorption sites are available for molecular interaction. Among the synthesized samples, the zeolite coded NaA–1.14–130 exhibits the highest surface area (127.48 m^2/g), suggesting that under these conditions, a balance between crystallinity and structural stability is achieved. This optimized synthesis condition therefore yields a zeolite with enhanced textural properties suitable for moisture adsorption applications.

Meanwhile, the pore size of the synthesized zeolite is indicated by the smaller pore diameter when the Si/Al ratio is higher. It is likely due to the greater strength of the silica bond, resulting in a reduced space in the crystal. The small pore size of the NaA zeolite allows the separation of small molecules based on their size differences, so that molecules such as H_2O (0.27 nm) are expected to be separated by the zeolite [41]. It occurs because the kinetics of N_2 adsorption on the NaA zeolite are too slow to reach equilibrium at the 77 K Isotherm point, so there is no regular isotherm. It occurs because the kinetic diameter of the nitrogen molecule (3.64 Å) is comparable to the effective channel diameter of NaA (around 4 Å), so that the nitrogen channel into NaA is closed [42].

The BJH-derived pore diameters reported in Table 4 were obtained from N_2 adsorption–desorption at 77 K. For NaA (LTA), N_2 diffusion into the framework apertures at 77 K is kinetically hindered because the kinetic diameter of N_2 (≈3.64 Å) is comparable to the LTA aperture (≈4.1 Å). Consequently, BJH analysis returns apparent mesopore/interparticle diameters (40–100 Å) that reflect inter-crystalline voids or external porosity rather than the intrinsic micropore channels of the LTA framework. To quantify true microporosity, it is recommended to use CO_2 physisorption at 273 K (with Dubinin–Radushkevich/density functional theory (DR/DFT analysis) for future work.

From the discussion above, the correlation between the Si/Al ratio, crystallinity, and adsorption performance of the synthesized zeolite A reveals an interdependent relationship governed by both framework composition and microstructural order. As shown in Table 2 and Table 4, an optimal Si/Al ratio of 1.14 yielded the highest crystallinity (97.00%) and a significantly larger surface area (127.48 m^2/g) compared to other ratios. This trend suggests that a balanced silicon-to-aluminum composition promotes the formation of a well-ordered zeolite framework, enhancing micropore connectivity and the availability of adsorption sites.

A lower Si/Al ratio (0.8) introduces an excess of aluminum, which increases the number of framework negative charges balanced by Na^+ cations. This condition favors nucleation but can lead to incomplete crystallization and the formation of amorphous phases, as observed in SEM images (characterized by a rounded cube morphology). The partial amorphicity reduces effective surface area and pore accessibility, thereby limiting adsorption performance. Conversely, a higher Si/Al ratio (1.8) increases the proportion of silica, which strengthens Si–O–Si bonds and reduces framework charge density. Although this makes the structure more hydrophobic and thermally stable, excessive silica leads to the formation of dense, less-porous regions that hinder water diffusion into the zeolite pores. The highest crystallinity and surface area were obtained at Si/Al = 1.14 and 130 °C, confirming that crystallinity enhances structural regularity and the number of accessible pores for moisture uptake. Therefore, the synergistic effect of a moderate Si/Al ratio and optimal synthesis temperature promotes both the structural and functional properties required for efficient water adsorption in zeolite A.

The Analysis of Zeolite Mass%

The XRF analysis was conducted to determine the mass percentage composition at various temperatures and Si/Al ratios, as shown in Table 5. From the table, the main composition consists of the elements Na, Al, and Si, with a small component of Ca. The components in each sample indicate the presence of elements that contribute to the formation of the zeolite structure. It demonstrates that the synthesized zeolite conforms to the characteristics of zeolite A, as established in research [43].

Moisture Adsorption Application Using a Humidity Chamber

Zeolites with optimum conditions based on different Si/Al ratios and temperatures were used for H_2O vapor adsorption applications. Table 6 shows the adsorption capacity of zeolite and molecular sieve in seconds. The adsorption capacity is expressed in parts per million by volume (ppmv) to determine the water content absorbed in the chamber. The average adsorption capacity of zeolite at 5 min was 0.188 ppmv, while that of molecular sieve was 1.101 ppmv. However, the adsorption measurement was only conducted up to 10 min, as the gas in the humidity chamber was already fully depleted beyond this point. Therefore, additional time points could not be recorded, and the available data were insufficient to construct a reliable kinetic or breakthrough curve. The synthesized zeolite demonstrates a lower moisture adsorption capacity than the commercial molecular sieve. The limited diffusion of water molecules through narrower pores and the reduced number of active adsorption sites on the surface likely restrict the overall uptake efficiency.

The drastic decrease in adsorption capacity observed at the 10th min can be attributed to competitive desorption and re-equilibration of water molecules within the zeolite micropores. During the initial adsorption phase (first 5 min), the zeolite's surface and accessible micropores rapidly adsorb H_2O molecules due to the strong electrostatic interaction between the water dipoles and the Na^+ cations located in the zeolite framework. However, as adsorption sites become saturated, a dynamic equilibrium begins to form between adsorbed and gas-phase water molecules. At this stage, localized temperature increases may occur inside the pores due to the exothermic nature of adsorption. The release of heat slightly elevates the zeolite's surface temperature, which can induce thermal desorption of weakly bound water molecules from less energetically favorable sites (e.g., external surfaces and pore entrances). Moreover, capillary condensation and subsequent pressure fluctuations in the humidity chamber may alter the partial pressure of water vapor, temporarily shifting the equilibrium toward desorption. Another possible factor is restricted diffusion within narrow pores (≈53 Å), where molecular back-diffusion becomes significant once the adsorption front stabilizes. This limitation slows the penetration of new water molecules into the inner pores,

Table 5. Mass percentage of zeolite

Sample	Mass (%)			
	Na_2O	Al_2O_3	SiO_2	CaO
NaA–0.80–70	32.1900	35.8400	31.7700	0.1610
NaA–1.14–70	32.0300	34.3700	33.3600	0.0227
NaA–1.80–70	31.7400	33.7100	34.2800	0.0171
NaA–0.80–100	65.7100	20.5400	13.4400	0.0339
NaA–1.14–100	35.3600	34.6100	29.8300	0.0148
NaA–1.80–100	31.0400	34.8400	33.8200	0.0187
NaA–0.80–130	66.0300	19.1100	14.4700	0.0381
NaA–1.14–130	54.4700	25.0100	20.2700	0.0274
NaA–1.80–130	34.8100	32.7200	32.2500	0.0181
Molecular sieve ref.	16.2300	40.6500	34.1400	7.7700

Table 6. The application of zeolite as a humidity absorber in a humidity chamber

5th min				
Sample code	A1	A2	MA1	MA2
Initial mass (g)	1.050	1.045	1.277	1.277
Final mass (g)	1.063	1.060	1.314	1.315
Adsorption capacity (%)	1.238	1.435	2.897	2.976
ppmv	0.161	0.215	1.072	1.131
10th min				
Sample code	A1	A2	MA1	MA2
Initial mass (g)	1.063	1.060	1.314	1.315
Final mass (g)	1.064	1.061	1.316	1.316
Adsorption capacity (%)	0.094	0.094	0.152	0.076
ppmv	0.000	0.000	0.000	0.000

Note: A1, A2 = Zeolite sample 1 and 2; MA1, MA2 = molecular sieve 1 and 2

while surface-bound water desorbs more readily, causing a net reduction in measurable adsorption capacity. Similar desorption–adsorption equilibria have been reported for zeolite 4A and 13X under cyclic moisture-loading conditions [14-15].

Although the synthesized zeolite A demonstrated a lower adsorption capacity (0.188 ppmv) than the commercial molecular sieve (1.101 ppmv), several factors can explain this performance gap. First, the specific surface area of the synthesized zeolite (127.48 m^2/g) is less than half that of the commercial molecular sieve (288.21 m^2/g), indicating fewer available adsorption sites. This reduced surface area may result from partial framework collapse or incomplete development of micropores during the hydrothermal synthesis stage, particularly at higher temperatures that can promote sintering. Second, while the synthesized zeolite exhibited high crystallinity (97%), minor amorphous phases observed in SEM images suggest incomplete crystallization, which can block or narrow pore channels, restricting gas diffusion. Third, particle size also plays a crucial role. SEM micrographs revealed particle sizes ranging from 0.5 to 8.0 µm, whereas commercial molecular sieves typically exhibit smaller, more uniform crystals that enhance diffusion kinetics and surface accessibility. Larger or irregular particles in the synthesized sample may hinder the rapid penetration of H_2O molecules into internal pores. Finally, diffusion limitations associated with smaller effective pore diameters (≈53 Å for the synthesized zeolite versus ≈170 Å for the commercial molecular sieve) can further reduce adsorption efficiency. The narrower pores impede the transport of water molecules, particularly under high humidity or pressure conditions. Together, these factors—limited surface area, partial amorphicity, larger particle size, and restricted pore diffusion—contribute to the observed lower adsorption capacity. Future optimization of synthesis parameters, such as hydrothermal duration, pH control, and post-synthesis activation, could help overcome these limitations and narrow the performance gap. Future work will focus on extended adsorption studies, including isotherm and regeneration analysis, using a continuous flow system.

■ CONCLUSION

This study successfully synthesized zeolite intended for application as a moisture absorber in the downstream oil production process. The zeolite was prepared using the hydrothermal method with a Si/Al ratio of 1.14 at 130 °C. The results confirmed that the synthesized material corresponds to zeolite A (LTA-type), composed primarily of Na, Al, Si, and O, with a crystallinity of approximately 97%, as indicated by the XRD pattern and supported by the XRF elemental composition. The SAA revealed that the synthesized zeolite possesses a specific surface area of 127.48 m^2/g, a pore volume of 0.17 cm^3/g, and an average pore diameter of 53 Å. When compared with a commercial molecular sieve, which exhibits a higher surface area of 288.2 m^2/g, a similar pore volume, and a larger average pore diameter of 170 Å, it becomes evident that the synthesized zeolite has a more compact structure with smaller pores and fewer accessible adsorption sites. Therefore, further studies are needed to optimize the hydrothermal duration, pH control, and post-synthesis activation.

■ ACKNOWLEDGMENTS

The authors gratefully acknowledge the Research and Technology Innovation, Pertamina, Indonesia, for funding this research.

■ CONFLICT OF INTEREST

There was no conflict of interest in this article.

■ AUTHOR CONTRIBUTIONS

Meyliana Wulandari wrote the manuscript, Nesya Juniar conducted the experiment and calculations, Stella Jovita assisted with the ImageJ software, Nofrizal and Pandian Bothi Raja revised the manuscript, and Wawan Rustyawan supervised the research. All authors agreed to the final version of this manuscript.

■ REFERENCES

[1] Wulandari, M., Nofrizal, N., Impey, S., Georgarakis, K., Raja, P.B., and Hussin, M.H., 2024, The effect of corrosion inhibitor on X-65 steel weldment in high

flow rate conditions, *Case Stud. Chem. Environ. Eng.*, 10, 100868.

[2] Wulandari, M., Zahratussaadah, Z., Nofrizal, N., Raja, P.B., and Andreas, A., 2023, Black tea waste as corrosion inhibitor for carbon steel in 0.5 M HCl medium, *Indones. J. Chem.*, 23 (6), 1664–1675.

[3] Nofrizal, N., Wulandari, M., Impey, S., Georgarakis, K., Papanikolaou, M., and Raja, P.B., 2024, An experimental and simulation screening of X-65 steel weldment corrosion in high flow rate conditions, *Mater. Today Commun.*, 39, 108793.

[4] Wu, L., Geng, W., Gao, L., Chen, J., and Zhao, H., 2017, Study of gas dehydration process by ionic liquid method in a rotating packed bed, *Energy Fuels*, 31 (12), 13400–13405.

[5] Zendehboudi, A., Angrisani, G., and Li, X., 2018, Parametric studies of silica gel and molecular sieve desiccant wheels: Experimental and modeling approaches, *Int. Commun. Heat Mass Transfer*, 91, 176–186.

[6] Azhagapillai, P., Khaleel, M., Zoghieb, F., Luckachan, G., Jacob, L., and Reinalda, D., 2022, Water vapor adsorption capacity loss of molecular sieves 4A, 5A, and 13X resulting from methanol and heptane exposure, *ACS Omega*, 7 (8), 6463–6471.

[7] Lin, R., Ladshaw, A., Nan, Y., Liu, J., Yiacoumi, S., Tsouris, C., DePaoli, D.W., and Tavlarides, L.L., 2015, Isotherms for water adsorption on molecular sieve 3A: Influence of cation composition, *Ind. Eng. Chem. Res.*, 54 (42), 10442–10448.

[8] Allanas, E., Rahman, A., Arlin, E., and Prasetyanto, E.A., 2021, Study surface area and pore size distribution on synthetic zeolite X using BET, BJH and DFT methods, *J. Phys.: Conf. Ser.*, 2019 (1) 12094.

[9] Moura, P.A.S., Ferracine, E.D.S., Rodríguez-Aguado, E., Maia, D.A.S., Melo, D.C., Valencia, S., Cardoso, D., Rey, F., Bastos-Neto, M., and Rodríguez-Castellón, E., 2024, Assessment of the stability of LTA zeolites under natural gas drying TSA conditions, *Catal. Today*, 427, 114410.

[10] Khaleque, A., Alam, M.M., Hoque, M., Mondal, S., Haider, J., Xu, B., Johir, M.A.H., Karmakar, A.K., Zhou, J.L., and Ahmed, M.B., 2020, Zeolite synthesis from low-cost materials and environmental applications: A review, *Environ. Adv.*, 2, 100019.

[11] Qi, K., Gao, L., Li, X., and He, F., 2023, Research progress in gas separation and purification based on zeolitic materials, *Catalysts*, 13 (5), 855.

[12] Ackley, M.W., Rege, S.U., and Saxena, H., 2003, Application of natural zeolites in the purification and separation of gases, *Microporous Mesoporous Mater.*, 61 (1-3), 25–42.

[13] Sudibandriyo, M., and Putri, F.A., 2020, The effect of various zeolites as an adsorbent for bioethanol purification using a fixed bed adsorption column, *Int. J. Technol.*, 11 (7), 1300–1308.

[14] Nascimento, B.O., dos Santos, B.F., Maia, D.A.S., de Melo, D.C., Vilarrasa-Garcia, E., Torres, A.E.B., Bastos-Neto, M., and Azevedo, D.C.S., 2021, Water adsorption in fresh and thermally aged zeolites: Equilibrium and kinetics, *Adsorption*, 27 (7), 1043–1053.

[15] Wynnyk, K.G., Hojjati, B., and Marriott, R.A., 2018, High-pressure sour gas and water adsorption on zeolite 13X, *Ind. Eng. Chem. Res.*, 57 (45), 15357–15365.

[16] Wynnyk, K.G., Hojjati, B., Pirzadeh, P., and Marriott, R.A., 2017, High-pressure sour gas adsorption on zeolite 4A, *Adsorption*, 23 (1), 149–162.

[17] Hejjaj, C., Aghzzaf, A.A., Scharnagl, N., Makha, M., Dahbi, M., Zheludkevich, M.L., Hakkou, R., and Fischer, C.B., 2021, Effect of 6-aminohexanoic acid released from its aluminum tri-polyphosphate intercalate (ATP-6-AHA) on the corrosion protection mechanism of steel in 3.5% sodium chloride solution, *Corros. Mater. Degrad.*, 2 (4), 666–677.

[18] Sukchit, D., Prajuabsuk, M., Lumlong, S., Inntam, C., Punkvang, A., Wattanarach, S., Thavorniti, P., Jongsomjit, B., Wongyai, K., Gleeson, D., Shanmugam, P., Boonyuen, S., and Pungpo, P., 2025, Synthesis and characterization of zeolite a from industrial fly ash as a green, cost-effective Cd^{2+}

and Pb^{2+} adsorbent for wastewater applications, *ACS Omega*, 10 (6), 5981–5992.

[19] Al-Jubouri, S.M., Sabbar, H.A., Waisi, B.I., and Lafta, H.A., 2019, Effect of synthesis parameters on the formation 4A zeolite crystals: Characterization analysis and heavy metals uptake performance study for water treatment, *Desalin. Water Treat.*, 165, 290–300.

[20] Qiang, Z., Shen, X., Guo, M., Cheng, F., and Zhang, M., 2019, A simple hydrothermal synthesis of zeolite X from bauxite tailings for highly efficient adsorbing CO_2 at room temperature, *Microporous Mesoporous Mater.*, 287, 77–84.

[21] Xiong, Y., Lu, G., Wang, Y., and Sun, Q., 2019, Synthesis and influence factors study of 4A molecular sieve via halloysite, *J. Electron. Mater.*, 48 (12), 7756–7761.

[22] Mintova, S., and Barrier, N., 2016, *Verified Syntheses of Zeolitic Materials*, International Zeolite Association, Napoli, Italy.

[23] Wulandari, M., Sampaleng, L.V.M., Shalihah, M.S., Razak, S., Sofyan, M.I., Ndruru, S.T.C.L., Kartini, R., Nofrizal, N., Suwardiyanto, S., and Raja, P.B., 2025, Application of hydrolyzed chitosan as an alternative shale inhibitor polyamine in high-pressure and high-temperature water-based mud, *Mater. Today Commun.*, 49, 114075.

[24] Tarani, E., Arvanitidis, I., Christofilos, D., Bikiaris, D.N., Chrissafis, K., and Vourlias, G., 2023, Calculation of the degree of crystallinity of HDPE/GNPs nanocomposites by using various experimental techniques: A comparative study, *J. Mater. Sci.*, 58 (4), 1621–1639.

[25] Marguí, E., and Queralt, I., 2024, "Sample Preparation for X-Ray Fluorescence Analysis" in *Encyclopedia of Analytical Chemistry*, John Wiley & Sons, Hoboken, New Jersey, US.

[26] Wulandari, M., Aulia, G.F., Rustyawan, W., Nofrizal, N., Suwardiyanto, S., Prasetyoko, D., and Raja, P.B., 2024, Hydroisomerization of *n*-dodecane over zeolite socony mobile-48-γ-Al_2O_3 supported platinum catalyst: Insight into platinum concentration and reaction temperature, *Case Stud. Chem. Environ. Eng.*, 10, 100789.

[27] Mallada, R., 2015, "Hydrothermal Synthesis of Zeolite" in *Encyclopedia of Membranes*, Eds. Drioli, E. and Giorno, L., Springer Berlin Heidelberg, Berlin, Heidelberg, 1005–1006.

[28] Ke, G., Shen, H., and Yang, P., 2019, Synthesis of X-zeolite from waste basalt powder and its influencing factors and synthesis mechanism, *Materials*, 12 (23), 3895.

[29] Derbe, T., Temesgen, S., and Bitew, M., 2021, A short review on synthesis, characterization, and applications of zeolites, *Adv. Mater. Sci. Eng.*, 2021 (1), 6637898.

[30] Grand, J., Awala, H., and Mintova, S., 2016, Mechanism of zeolites crystal growth: New findings and open questions, *CrystEngComm*, 18 (5), 650–664.

[31] Saynik, P.B., and Moholkar, P., 2022, Influence of different salts of alkali and alkaline earth metals on the pyrolysis of *Prosopis juliflora*, *Biofuels, Bioprod. Biorefin.*, 16 (4), 1038–1049.

[32] Anbia, M., Koohsaryan, E., and Borhani, A., 2017, Novel hydrothermal synthesis of hierarchically-structured zeolite LTA microspheres, *Mater. Chem. Phys.*, 193, 380–390.

[33] Treacy, M.M., and Higgins, J., 2001, *Collection of Simulated XRD Powder Pattern for Zeolites*, Elsevier Science, Amsterdam, Netherlands.

[34] Liu, Z., Li, S., Li, L., Wang, J., Zhou, Y., and Wang, D., 2019, One-step high efficiency crystallization of zeolite A from ultra-fine circulating fluidized bed fly ash by hydrothermal synthesis method, *Fuel*, 257, 116043.

[35] Nguyen, D.K., Dinh, V.P., Dang, N.T., Khan, D.T., Hung, N.T., and Thi Tran, N.H., 2023, Effects of aging and hydrothermal treatment on the crystallization of ZSM-5 zeolite synthesis from bentonite, *RSC Adv.*, 13 (30), 20565–20574.

[36] Bosnar, S., Bronić, J., Brlek, Đ., and Subotić, B., 2011, Chemically controlled particulate properties of zeolites: Towards the face-less particles of zeolite A. 2. Influence of aluminosilicate batch concentration and alkalinity of the reaction mixture (hydrogel) on the size and shape of zeolite A

crystals, *Microporous Mesoporous Mater.*, 142 (1), 389–397.

[37] Li, Q., Zhang, Y., Cao, Z., Gao, W., and Cui, L., 2010, Influence of synthesis parameters on the crystallinity and Si/Al ratio of NaY zeolite synthesized from kaolin, *Pet. Sci.*, 7 (3), 403–409.

[38] Fischer, R.X., Šehović, M., Baur, W.H., Paulmann, C., and Gesing, T.M., 2012, Crystal structure and morphology of fully hydrated zeolite Na-A, *Z. Kristallogr. - Cryst. Mater.*, 227 (7), 438–445.

[39] Sayehi, M., Delahay, G., and Tounsi, H., 2022, Synthesis and characterization of ecofriendly materials zeolite from waste glass and aluminum scraps using the hydrothermal technique, *J. Environ. Chem. Eng.*, 10 (6), 108561.

[40] Liu, G., Lin, Y., Zhang, L., Zhang, M., Gu, C., Li, J., Zheng, T., and Chai, J., 2024, Preparation of NaA zeolite molecular sieve based on solid waste fly ash by high-speed dispersion homogenization-assisted alkali fusion-hydrothermal method and its performance of ammonia-nitrogen adsorption, *J. Sci.: Adv. Mater. Devices*, 9 (1), 100673.

[41] Kazemimoghadam, M., 2017, Multi-stage synthesis of nanopore NaA zeolite membranes for separation of water/ethanol mixtures, *Int J Res Eng Innovation*, 6, 42–46.

[42] Mehio, N., Dai, S., and Jiang, D., 2014, Quantum mechanical basis for kinetic diameters of small gaseous molecules, *J. Phys. Chem. A*, 118 (6), 1150–1154.

[43] Yusuf, E.O., Efeovbokhan, V.E., and Babalola, R., 2019, Development and characterization of zeolite-A from Elefun kaolin, *J. Phys.: Conf. Ser.*, 1378 (3), 32016.